Alloying and strain relaxation effects on spin-reorientation transitions in $Co_xNi_{1-x}/Cu_3Au(100)$ ultrathin films

W. C. Lin, B. Y. Wang, and Y. W. Liao
Department of Physics, National Taiwan University, Taipei 106, Taiwan
and Institute of Atomic and Molecular Sciences, Academia Sinica, Taipei, Taiwan

Ker-Jar Song*
Institute of Atomic and Molecular Sciences, Academia Sinica, Taipei, Taiwan

Minn-Tsong Lin†
Department of Physics, National Taiwan University, Taipei 106, Taiwan
and Institute of Atomic and Molecular Sciences, Academia Sinica, Taipei, Taiwan
(Received 22 October 2004; revised manuscript received 28 January 2005; published 25 May 2005)

The crystalline structure and the magnetic properties of $Co_xNi_{1-x}/Cu_3Au(100)$ films were characterized as functions of thickness and alloy composition. No apparent alloy effect on the crystalline structure was observed with x up to 11%. As the film thickness increases above ~8 monolayers (ML), the films clearly exhibited a progressively more relaxed structure. Due to the strain relaxation, both the first and the second spin-reorientation transitions (SRT) occurred within 20 ML. The thickness region with perpendicular magnetization was strongly reduced by increasing the Co concentration. For $x > 10\%$, no SRT was observed. By combining both the alloy effect and the strain relaxation effect, the SRT boundaries in the phase diagram can be described in a phenomenological model on the basis of magnetoelastics.

DOI: 10.1103/PhysRevB.71.184413 PACS number(s): 75.70.Ak, 75.50.Bb, 78.20.Ls

I. INTRODUCTION

In magnetic ultrathin films, the reducing of dimensionality leads to many interesting properties different from bulk materials. One of them is the spin-reorientation transition (SRT), which implicates switching of the magnetic easy axis with variation of the thickness, the temperature, or the crystalline structure of the film.[1,2] For example, the magnetization switches from perpendicular to in-plane direction as the film thickness increases for systems, such as Co/Au(111),[3] Fe/Cu(100),[4] and $Fe/Cu_3Au(100)$.[2,5,6] In contrast, Ni/Cu(100) films reveal *inverse* SRT at about 7–10 monolayer (ML),[1,7–11] in which the magnetization switches from the in-plane to perpendicular direction with increasing thickness. This inverse SRT originates from the strain-induced magnetoelastic anisotropy, which prefers the perpendicular magnetization. At a higher thickness, the strain gradually relaxes and the easy axis goes back to in-plane again.[8] In the past decades, the phenomenological Néel-type model has been used successfully to describe the thickness-dependent SRT in various systems, and many experimental studies have aimed to characterize the SRT from the view of this phenomenological model. However, in experiments studying thickness-dependent SRT, one may usually get only one critical thickness (d_c) to characterize the SRT phenomenon. Since spin orientation is the result of the competition between many different magnetic anisotropies, such as magnetoelastic anisotropy, shape anisotropy, etc., only one or two data points of d_c is not adequate to tell us about the evolution of various magnetic anisotropy. Due to this point, many binary alloy systems, such as Fe-Co/Cu(100),[12] Fe-Ni/Cu(100),[13,14] and Co-Ni/Cu(100),[15] have been prepared to characterize the alloy effect on the SRT behavior. The SRT behavior reveals a clear boundary in the magnetic phase diagram with the variation of the film thickness and the alloy concentration. It can further be used to determine the contributions from various magnetic anisotropies with little ambiguity. Presumably, the magnetic anisotropy varies with the alloy concentration as a result of the modification to the electronic structure which is outside the scope of this manuscript at this point. Such an observation can be compared with several theoretical calculations about the anisotropy of 3*d* alloys that have been reported recently.[16–18]

In the case of $Co_xNi_{1-x}/Cu(100)$, due to the small lattice mismatch and the small strain, the film needs to be very thick in order for strain relaxation to occur. Thus, the second SRT happens at very large thickness and is easily influenced by the small changes in the growth condition. As there is larger scatter in the measured critical thickness for the second SRT, it is difficult to analyze the alloy effect on this boundary. Hence all the efforts of previous studies have been focused on the alloy effect on the first SRT.[13–15] It would be nice to have the information of the alloy effect on the second SRT, because it can bring us more details about the alloy effects on the magnetic anisotropies, especially the magnetoelastic anisotropy. In this experiment, we choose $Cu_3Au(100)$ as the substrate, instead of Cu(100). Due to the larger mismatch of the $Ni/Cu_3Au(100)$ system [$Ni/Cu_3Au(100)$: −6.1%, Ni/Cu(100): −2.6%], strain relaxation starts to occur with thinner films. Both the inverse SRT and the second SRT occur within 20 ML. Therefore, the alloy effect on the second SRT boundary can be characterized completely in the $Co_xNi_{1-x}/Cu_3Au(100)$ system. With both SRT boundaries in this system, we can extract more information on the thick-

ness evolution and the alloy modification of the various magnetic anisotropy terms. Due to the relaxation of strain, the surface anisotropy of films is no longer constant in the thickness region of the second SRT. A strain-dependent term must be considered in surface anisotropy, called the surface magnetoelastic anisotropy.[8] Therefore, the alloy effect on the second SRT boundary not only helps us to reconfirm the previous experimental and theoretical results of volume magnetoelastic anisotropy but also gives further information about the alloying effect on the surface magnetoelastic anisotropy.

II. EXPERIMENT

This experiment was performed in an ultrahigh vacuum (UHV) chamber with the base pressure $<2\times10^{-10}$ Torr. The $Cu_3Au(100)$ single crystal with miscut $\approx0.1°$ was cleaned by cycles of 3 keV Ne-ion sputtering. After cleaning, the substrate was annealed at 765 K for 5 min, and then at 645 K for 30 min to get smooth and well-ordered surface. The well-ordered $c2\times2$ structure[2,5] was verified by low-energy electron diffraction (LEED). Co_xNi_{1-x} alloy films were prepared by co-deposition while the substrate is at 300 K. During the evaporation, the pressure was better than 3×10^{-10} Torr and the growth was monitored in real time by medium-energy electron diffraction (MEED) with a beam energy of 5 keV and grazing angle of 1°. From the periodicity of MEED oscillation, the deposition rate was calibrated and controlled precisely. We calibrated the deposition rates of Co and Ni individually from the MEED oscillation of pure Co and pure Ni films. Then, the same deposition rates of Co and Ni were repeated by keeping the same deposition parameters during the co-deposition of Co–Ni alloy films. The repeat of Co and Ni deposition rates was very reliable and can be checked by: Deposition rate of Co–Ni alloy films = deposition rate of Co + deposition rate of Ni. Besides, as shown in our previous paper,[19] Auger electron spectroscopy (AES) also helped us to confirm the Co concentration.

Measurement of LEED and LEED-current/voltage (I/V) curves was performed to identify the morphology and the crystalline structure. From the LEED-I/V curve, the average vertical interlayer distance ($a_\perp$) was determined using the kinematic approximation.[15,19] Magnetic properties of the films were monitored by magneto-optical Kerr effect (MOKE). The MOKE measurement was performed *in situ* in both the longitudinal and the polar geometry using modulation and lock-in technique.

III. RESULTS

A. Growth mode

Figure 1 shows the MEED intensity of various films grown at 300 K as a function of deposition time. The MEED curves of the alloy films with x up to 11% have roughly the same features as that of the pure Ni film. From this result, and the similar face-centered-cubic (fcc) lattice constants of Co and Ni (Co: 1.77 Å, Ni: 1.76 Å), it is reasonable to conclude that small Co concentration does not cause apparent changes of the growth mode. In Fig. 1, clear oscillations

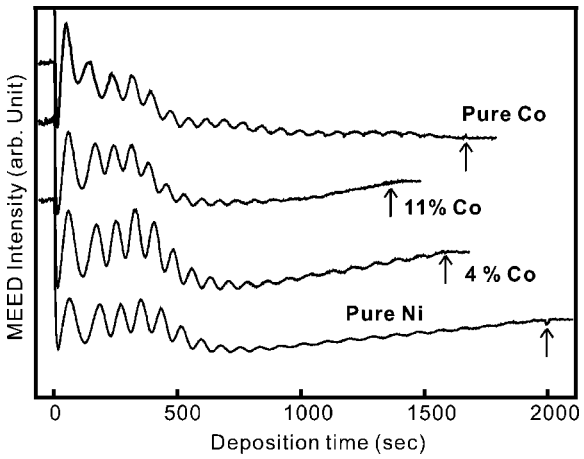

FIG. 1. MEED intensity oscillation of various ultrathin Co–Ni alloy films grown at room temperature on $Cu_3Au(100)$.

persists until 5 ML and after that, the amplitude of oscillation quickly reduces to smaller values. These small-amplitude oscillations, which continue for more than 20 ML and gradually disappear, also help us to calibrate the film thickness precisely even at higher coverage. The evolution of oscillation intensity described above clearly shows the transition of growth mode from layer-by-layer to island growth at 5–6 ML. After the transition to island growth, the surface becomes rougher than the condition under layer-by-layer growth (0–5 ML). As indicated in a previous study of the MEED and scanning tunneling microscopy experiments for $Fe/Cu_3Au(100)$,[5] the reduced peak intensity of MEED oscillation is connected with the enhanced roughness in island growth. In addition, Matthes *et al.*[20] did not observe so many oscillations in $Ni/Cu_3Au(100)$. We also tried to check it by changing the grazing angle of the electron beam and, in fact, we can reproduce the same data as shown by Matthes with a larger grazing angle of 4°. Thus, the growth condition in this work should be similar to the previous study.

Furthermore, as compared with Ni/Cu(100),[15] Ni films on $Cu_3Au(100)$ revealed similar layer-by-layer growth, although the mismatch of $Ni/Cu_3Au(100)$ (-6.1%) is much larger than that of Ni/Cu(100) (-2.6%). In our AES analysis, Au segregation could be seen in Ni films on $Cu_3Au(100)$ grown at 300 K. Similar results also have been observed by Braun *et al.*[21] and they suggested that the segregated Au seems to help layer-by-layer growth in $Ni/Cu_3Au(100)$ at 300 K.

B. Crystalline structure

The crystalline structure of the alloy films after being cooled down to 100 K was characterized by LEED and LEED-I/V measurements. Structure-wise, for alloy films of the same thickness, no significant difference appeared with the variation of the alloy composition ($x\leqslant11\%$). This can be attributed to the similar fcc lattice constant of Co and Ni. Since the lattice mismatches of Co and Ni on $Cu_3Au(100)$ are -5.6% and -6.1%, respectively, a 10% alloy composition will induce only a 0.05% variation in lattice mismatch, and thus gives no significant effect on the crystalline structure.

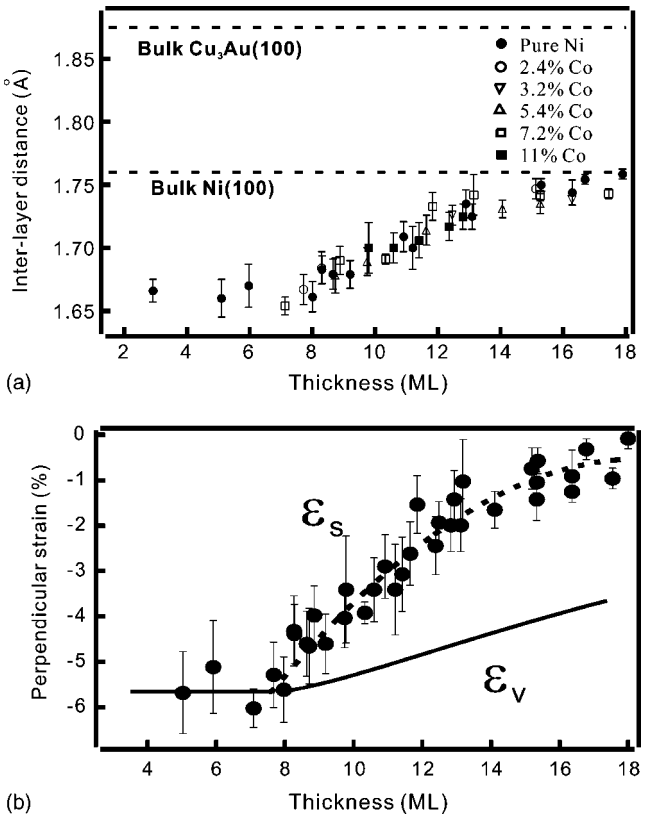

FIG. 2. (a) Vertical interlayer distance ($a_\perp$) of various $Co_xNi_{1-x}/Cu_3Au(100)$ alloy films. $a_\perp$ relaxes from highly compressed lattice (1.66 ± 0.02 Å) to almost bulk structure (1.76 ± 0.02 Å) with the increasing of thickness. There is no apparent difference in the relaxation process of films with different alloy composition. (b) Vertical strain calculated from the $a_\perp$ in (a). The dashed line is a curve fitting [$\varepsilon_s(d)$] of all the data points and the solid line is the "average strain" $\varepsilon_v(d)$ of the film.

Therefore, the effect of alloying on the crystalline structure can be neglected in the following discussion.

On the other hand, the energy of the peaks in LEED-I/V curves shifted drastically with the variation of the film thickness. Figure 2(a) shows the vertical interlayer distance $a_\perp$ obtained from LEED-I/V curves of various alloy films.[19] The dashed lines indicate the $a_\perp$ of bulk Ni(100) and $Cu_3Au(100)$.[2,5,19] The $a_\perp$ of bulk $Cu_3Au(100)$ is deduced from the LEED-I/V of the substrate and its value is 1.87 ± 0.02 Å, which is consistent with the literature. Because of the large negative mismatch, the films sustain a tensile stress in the film plane and the $a_\perp$ of the alloy film is compressed as compared with bulk Ni. In Fig. 2(a), $a_\perp$ keeps nearly invariant at about 1.66 Å until 8 ML and then gradually increased to ~1.75 Å with thickness up to 18 ML. In other words, the alloy films gradually relax to the bulk structure of Ni after 8 ML. From the *k*-space lattice measured by LEED images, the in-plane strain relaxation was also observed. However, due to the morphology-induced broadening of the spot profile, it is difficult to precisely characterize the in-plane strain relaxation. Unlike the drastic fcc-to-body-centered-cubic structural transition of $Fe/Cu_3Au(100)$ films,[2,6] the relaxation process of Co_xNi_{1-x} films was similar to the case of Fe/W(100)[22] in which pseudomorphic growth was observed during the deposition of the first 3 ML, strain relaxation occurred between 3–6 ML and only small residual strain existed after 6 ML. This thickness-dependent strain relaxation of $Co_xNi_{1-x}/Cu_3Au(100)$ films may induce the evolution of magnetic anisotropy, and thus leads to the second SRT. The related details will be discussed below.

The quickly reduced MEED oscillation at 5–6 ML in Fig. 1 implies the trend to an island growth. As the lateral relaxation is more likely to initiate at the island edges, it seems quite reasonable that in $Co_xNi_{1-x}/Cu_3Au(100)$ films, the strain relaxes after the appearance of island growth.

From $a_\perp$ of the various alloy films in Fig. 2(a), the vertical strain $\varepsilon_\perp$ as shown in Fig. 2(b) can be calculated by the following definition:[23]

$$\varepsilon_\perp = (a_\perp - a_b^{\mathrm{Ni}})/a_b^{\mathrm{Ni}}, \tag{1}$$

where a_b^{Ni} is the bulk lattice constant of Ni.

From the studies of Ha *et al.*,[23] the ratio of nickel in-plane to perpendicular strains is -1.18 ± 0.05, which is also very close to the value reported by Platow *et al.*[24] Thus, the in-plane strain $\varepsilon_\parallel$ can be estimated from the perpendicular strain $\varepsilon_\perp$ based on the ratio reported in previous papers:

$$\varepsilon_\parallel = -(1/1.18)\cdot\varepsilon_\perp. \tag{2}$$

Since the electron diffraction method can only give the average value of the $a_\perp$ near the surface, data points shown in Fig. 2(b) are assumed to be the strain of the top layer by neglecting the averaging effect from the mean-free path of low-energy electron. The dashed line in Fig. 2(b) is a curve fitting with an analytical function of Gaussian form to all the strain data.[25] Similar to other reports on Ni/Cu(100),[23] our data of strain relaxation do not follow the conventional $(1/d)$ form. From the stress measurement of other surface relaxation systems, such as Fe/W(100) studied by Enders *et al.*,[22] the total stress is the integration of the contributions from each individual layers and it keeps on increasing with the film thickness even after the strain relaxation. This suggests that even when the top layers of the film start to relax, the strain of the underlying layers might still remain locked in place. That is why the total stress keeps on increasing, but not dropping down during and after strain relaxation. Only the increasing rate of the total stress is reduced by the strain relaxation and finally the total stress saturates after total relaxation. From this picture of strain relaxation, the average strain of the film can be thus calculated, as shown by the solid line in Fig. 2(b), by adding up the strain of the individual layers from the dashed line and then divided by the total thickness:

$$\varepsilon_v(d) = (1/d)\cdot\int_0^d \varepsilon_s(t)\cdot dt, \tag{3}$$

where d is the film thickness, and ε_s is the surface strain obtained from experimental data of $a_\perp$. These dashed and solid lines shown in Fig. 2(b) represent thus the evolution of the surface strain $\varepsilon_s(d)$ and the average volume strain $\varepsilon_v(d)$, respectively, which later will be applied in the phenomenological model with magnetoelastic anisotropy.

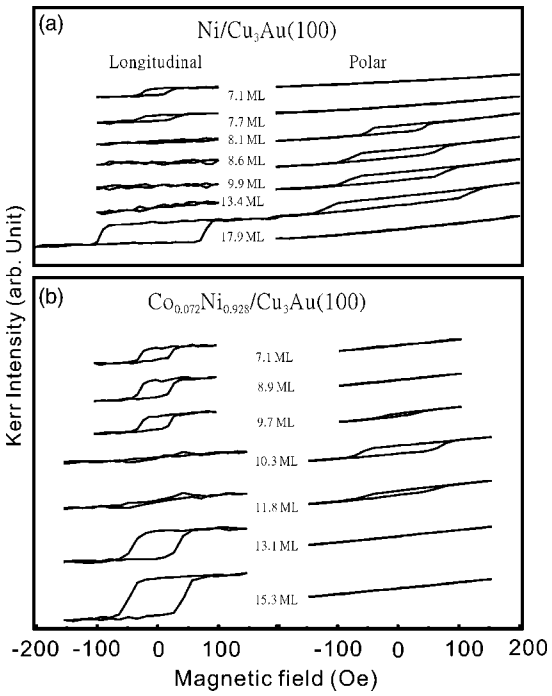

FIG. 3. Longitudinal and polar MOKE hysteresis loops of (a) $Ni/Cu_3Au(100)$ and (b) $Co_{0.072}Ni_{0.928}/Cu_3Au(100)$ films with different thickness. The measurement temperature is 100 K. In the two cases, both of the first SRT and the second SRT were observed.

C. Magnetic properties

Figure 3 shows the MOKE hysteresis loops of pure Ni and $Co_{0.072}Ni_{0.928}$ alloy films grown at room temperature on $Cu_3Au(100)$ in both longitudinal and polar geometry. The measurement was performed at 100 K. In pure Ni films, the easy axis switches from the in-plane to perpendicular direction at 7.7–8 ML (first SRT) and switches back again at higher thickness of ~17 ML (second SRT). Our data are similar to the report of Braunn *et al.*[21] on $Ni/Cu_3Au(100)$ films. They showed that between 8 and 12 ML, no signals were measured in longitudinal geometry, but in polar geometry. There are two possible reasons for the deviation of the SRT critical thickness. The first one is the differences in the preparation condition, especially the UHV environment and the substrate. Take Ni/Cu(100) for example, the critical thickness of the first SRT ranges from 7 to 10 ML due to the different preparation conditions in different groups.[1,7–11] The second possibility might be that Braun's MOKE data were taken from a wedge sample. The possible differences in magnetic domain and crystalline structure between a wedged sample and a uniform film may also influence the SRT behavior.

In Fig. 3(b), 7.2% Co delays the first SRT to higher coverage and shifts the second SRT to lower coverage. The same measurement was performed for alloy films with different Co concentration and thickness. All of the MOKE data are summarized as a phase diagram shown in Fig. 4. The empty and solid circles indicate the presence and absence of polar hysteresis loop, respectively. Clearly, the thickness region with

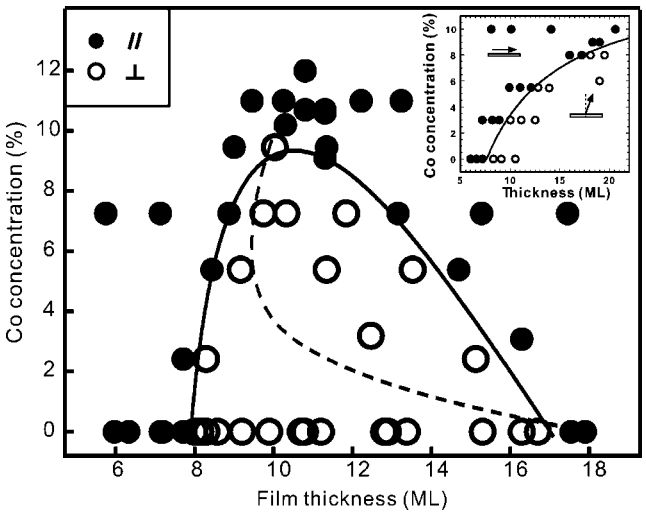

FIG. 4. Magnetic phase diagram of $Co_xNi_{1-x}/Cu_3Au(100)$ with respect to the film thickness and the alloy concentration. All of the films were grown at 300 K and the magnetic behavior was measured at 100 K. The empty and solid circles indicate the presence and absence of polar hysteresis signal, respectively. The solid line presents the fitted boundary. The dashed line indicates the bad fitting of the second SRT by taking $\varepsilon_s = \varepsilon_v$. For comparison, the inset shows our previous results of $Co_xNi_{1-x}/Cu(100)$.

perpendicular magnetization was gradually reduced with the increasing of the Co concentration. As the Co concentration increases from 0% to 9.5%, the critical thickness of the first and the second SRT varies from 7.8 ML to 9.8 ML and from 17 ML to 10.5 ML, respectively. When the Co concentration is larger than 10%, no SRT can be observed.

In comparison with our previous study on $Co_xNi_{1-x}/Cu(100)$ (inset of Fig. 4), the $Co_xNi_{1-x}/Cu_3Au(100)$ system reveals a very different SRT phase diagram. First, the first SRT boundary was shifted from 7 to more than 20 ML by 9% Co in Cu(100) system. However, in the case of $Cu_3Au(100)$ system, the shift is only ~2 ML by 9.5% Co. Apparently, the alloy effect on the first SRT is not as strong in $Cu_3Au(100)$ system as in Cu(100) system. Besides, in contrast to that only the first SRT boundary was observed in the Cu(100) system within 20 ML, the $Cu_3Au(100)$ system displays both SRT boundaries within 20 ML.

IV. PHENOMENOLOGICAL MODEL OF SRT

In the past decades, the phenomenological Néel-type model has been used successfully to describe the thickness-dependent SRT in various systems, and many experimental studies have aimed to characterize the SRT from the view of this phenomenological model. Considering only the lowest-order term, the perpendicular magnetic anisotropy per volume can be described as[15]

$$E = K_{\text{eff}} \cdot \sin^2 \theta, \tag{4}$$

$$K_{\text{eff}} = \frac{K_s}{d} + K_v = \frac{K_s}{d} + (K_{\text{me}} - 2\pi M^2), \tag{5}$$

where θ is the angle between the surface normal and the

orientation of the magnetization. d stands for the film thickness. $-2\pi M^2$ is the shape anisotropy and M denotes the magnetic moment density. K_{me} is the volume magnetoelastic anisotropy, which is the product of the volume magnetoelastic constant B_v and the average volume strain ε_v.

In Eq. (4), from the condition of minimum energy, the magnetization of the film prefers the perpendicular (in-plane) direction if $K_{\mathrm{eff}}>0$ (<0). Thus, SRT happens when K_{eff} changes signs and we can get the critical thickness d_c of SRT by solving $K_{\mathrm{eff}}=0$:

$$d_c = \frac{-K_s}{K_v} = \frac{-K_s}{(K_{\mathrm{me}} - 2\pi M^2)}. \tag{6}$$

This model has been applied to the first SRT of Ni/Cu(100).[9] It gives us the picture that the first SRT originates from a negative K_s and a large positive K_{me} ($>2\pi M^2$).

A. Alloy effect on SRT

Furthermore, we had found the experimental data of the first SRT boundary in $\mathrm{Co}_x\mathrm{Ni}_{1-x}$/Cu(100) can be reproduced by this model if we assume the magnetic moments M, the surface anisotropy K_s, and the volume magnetoelastic anisotropy K_{me} are linear function of the concentration x. Equation (6) is modified as

$$d_c = \frac{-2[xK_s^{\mathrm{Co}} + (1-x)K_s^{\mathrm{Ni}}]}{\{[xK_{\mathrm{me}}^{\mathrm{Co}} + (1-x)K_{\mathrm{me}}^{\mathrm{Ni}}]\} - 2\pi[xM^{\mathrm{Co}} + (1-x)M^{\mathrm{Ni}}]^2}. \tag{7}$$

The linear variation of magnetic moment has been measured by experiments as the Slater-Pauling curve.[26–28] The reason for the linear approximation of magnetic anisotropy originates from the small value of Co concentration x, and the consistent results of linear variation in previous experiments[14,15] and calculations.[16,18] Both in the experiments and calculations, the magnetic anisotropy of $\mathrm{Co}_x\mathrm{Ni}_{1-x}$ alloy is approximately a linear function of x, when x is small.

B. Strain relaxation effect on SRT

Besides the alloy system, Eq. (5) is extended to describe both of the first and the second SRT of Ni/Cu(100) by adding the surface magnetoelastic anisotropy and considering the strain relaxation as:

$$K_{\mathrm{eff}} = \frac{-(B_s\varepsilon_s + k_s^{\mathrm{cry}})}{d} + (B_v \cdot \varepsilon_v - 2\pi M^2), \tag{8}$$

where B_s is the surface magnetoelastic constant, and ε_s is the perpendicular strain at the surface. k_s^{cry} is the surface magnetocrystalline anisotropy, which is the strain-independent part of the surface anisotropy K_s due to spin-orbital coupling.

While studying the first SRT of Ni/Cu(100), no strain relaxation was observed ($\varepsilon_s=\varepsilon_v=$constant).[23,23] Therefore, $B_s\cdot\varepsilon_s$ can be combined with k_s^{cry} as a constant, which is independent of the film thickness [like K_s in Eq. (6)]. However, in considering the second SRT of Ni/Cu(100), strain relaxation happens with increasing thickness. Thus $B_s\varepsilon_s$ is no longer a constant and we need to separate $B_s\cdot\varepsilon_s$ and k_s^{cry} explicitly to take care of the thickness-dependent strain relaxation.

C. Alloy+strain relaxation effect on SRT

Since our data shown in Fig. 4 include both the alloy effect and the strain-relaxation-induced second SRT, It is straightforward to combine Eqs. (7) and (8) as

$$K_{\mathrm{eff}} = \frac{-(B_s\cdot\varepsilon_s + k_s)}{d} + \{[xK_{\mathrm{me}}^{\mathrm{Co}} + (1-x)K_{\mathrm{me}}^{\mathrm{Ni}}]\}\left(\frac{\varepsilon_v}{3.2\%}\right) - 2\pi[xM^{\mathrm{Co}} + (1-x)M^{\mathrm{Ni}}]^2, \tag{9}$$

$$d_c = \frac{-(B_s\cdot\varepsilon_s + k_s)}{\{[xK_{\mathrm{me}}^{\mathrm{Co}} + (1-x)K_{\mathrm{me}}^{\mathrm{Ni}}]\}\left(\frac{\varepsilon_v}{3.2\%}\right) - 2\pi[xM^{\mathrm{Co}} + (1-x)M^{\mathrm{Ni}}]^2}. \tag{10}$$

In the numerator, following the form of Eq. (8), a strain-related term is separated from the surface anisotropy. In the denominator, the volume magnetoelastic anisotropy K_{me} of the alloy films follows the same linear combination in Eq. (7), since Eq. (7) is good in describing the Co–Ni alloy films on Cu(100). The factor 3.2% in front of the K_{me} term is the correction for the different $\varepsilon_\perp$ of Ni/Cu(100) before relaxation.[23,24] Next, we need to determine B_s and k_s with the variation of alloy composition x. Since x ranges up to only 0.11, the undetermined parameters B_s and k_s are approximated as linear functions of x: $B_s(x)=B_{s0}+xB_{s1}$,$k_s(x)=k_{s0}+xk_{s1}$. By taking the two critical thickness of the first and the second SRT (d_{c1},d_{c2}) in pure Ni films into Eq. (10) (with $x=0$), we can solve the values of B_{s0} and k_{s0} from these two equations. Finally, only two parameters, B_{s1} and k_{s1}, need to be determined from fitting the SRT boundary of alloy films.

The last question is how to properly calculate the surface strain (ε_s) and the average volume strain (ε_v). In Bochi's report,[8] $\varepsilon_s=\varepsilon_v$ is assumed, which implies the strain relaxation in all layers of the film are the same. However, if $\varepsilon_v=\varepsilon_s$, one fails to describe the phase boundaries of SRT, as shown by the dashed line in Fig. 4. No matter what values of

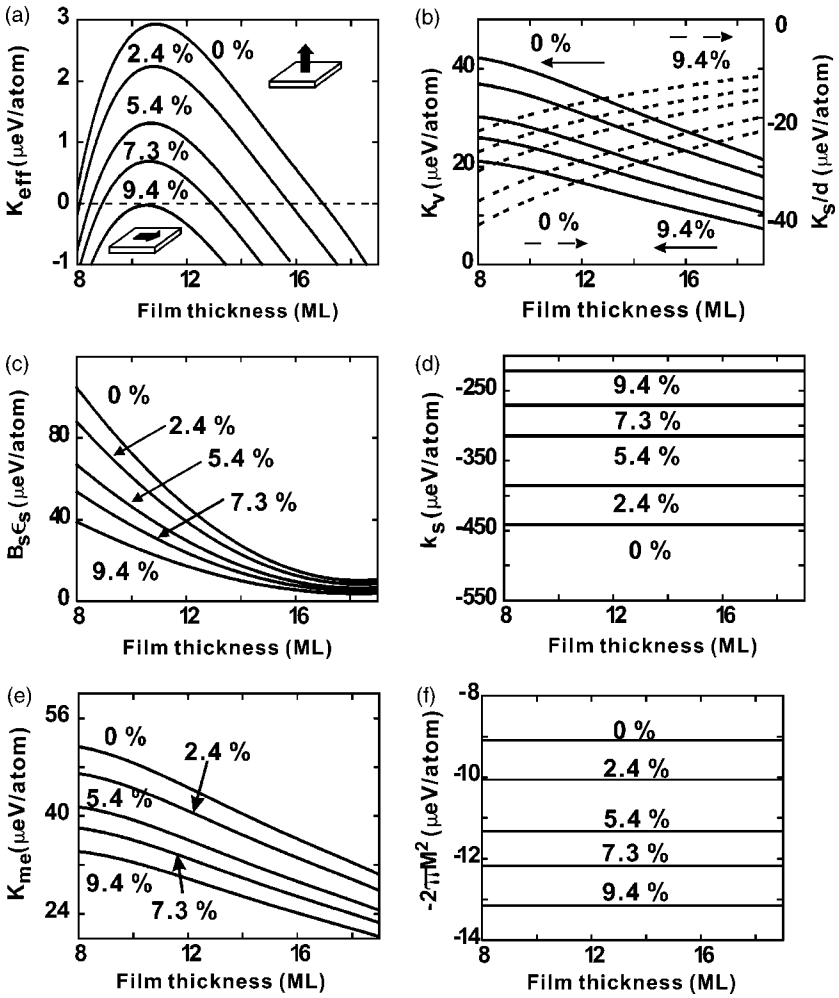

FIG. 5. Each curve is labeled by the concentration of Co. (a) K_{eff} of different Co_xNi_{1-x} alloy films. (b) Solid lines (left axis) are the surface contribution K_s/d, and dashed lines (right axis) are the volume contribution: K_v. (c)–(f) The surface magnetoelastic term ($B_s\varepsilon_s$), k_s, the volume magnetoelastic term (K_{me}), and the shape anisotropy ($-2\pi M^2$) of various alloy films, respectively.

B_{s1} and k_{s1} we choose, it is impossible to fit the second SRT boundary well.[29]

At the conclusion of the above attempt, we are forced to give up the assumption $\varepsilon_v=\varepsilon_s$. As mentioned in the section of the crystalline structure, it is compatible with the experimental data that individual layers in the film have a different degree of strain relaxation. Thus, the average volume strain ε_v can be determined by the definition of Eq. (3) [solid line in Fig. 2(b)] and is substituted into Eq. (10). The SRT boundary in the phase diagram can now be determined very well in this new model if $B_{s0}=-1950\pm200$ μeV/atom, $k_{s0}=-441\pm10$ μeV/atom, and properly choosing the fitting parameters: $B_{s1}=13000\pm5000$ μeV/atom, $k_{s1}=2340\pm200$ μeV/atom.[30] Note that, since we used the perpendicular strain in the Eq. (10), the value of B_s should be little deviated from that obtained with in-plane strain by a factor of Poisson's ratio ($\sim$1.18).[23,31]

According to the above picture of relaxation, although the further away from the interface, the better the strain is relaxed, the strain on the Ni–Cu_3Au(100) interface is supposed to be frozen in, and the surface magnetoelastic anisotropy for the Ni–Cu_3Au(100) interface should be independent of strain relaxation. The k_s of the surface anisotropy K_s thus includes not only the surface crystalline anisotropy, but also the surface magnetoelastic anisotropy for the Ni–Cu_3Au(100) interface related to the residual strain. This is also why we use k_s instead of k_s^{cry}. Besides in the case of Ni/Cu(100), Bochi *et al.*[8,31] also reported the B_s of Ni-vacuum surface$=-5174$ μeV/atom. Our $B_s(x=0)=B_{s0}=-1950\pm200$ μeV/atom is of the same sign and the same order as theirs.

V. DISCUSSION

With the parameters obtained in the last section, the K_{eff} with various Co concentrations is depicted in Fig. 5(a) as a function of thickness. Figure 5(b) reveals the competition between the surface contribution (K_s/d) and the volume contribution (K_v) in different alloy films. Figures 5(c)–5(f) show the thickness and the alloy evolution of distinct magnetic anisotropy terms in Eq. (9).

A. Strain-induced (thickness-dependent) SRT

The thickness and alloy-induced evolution of magnetic anisotropy from surface and volume contribution are shown in Fig. 5(b). At low coverages ($<$10 ML), the positive K_{me} and the decaying K_s/d (<0) result in the increasing tendency of K_{eff}. Thus, K_{eff} increases from negative to positive with thickness in Fig. 5(a), and the first SRT happens when K_{eff} crosses zero. After 10 ML, due to the strain-relaxation, K_{me} drops down quickly and becomes compatible with the decay-

TABLE I. Magnetic moments and anisotropies of Co and Ni.

	$K_{\mathrm{me}}(\mu\mathrm{eV/atom})$	$K_s(\mu\mathrm{eV/atom})$	$M(\mu_B)$	$-2\pi M^2(\mu\mathrm{eV/atom})$
Co/Cu(100)[26,27]	−73.8	−55.8	1.8	−90
Ni/Cu(100)[9,27]	29	−77	0.57	−9.1

ing K_s. Thus, although the surface anisotropy (<0) decays by $(1/d)$, it still can cover the positive volume contribution. Then, K_{eff} goes back to be negative again. This is the second SRT. At a much higher thickness, K_{me} and K_s drop to zero due to the strain relaxation and the $1/d$ decay. Then, the shape anisotropy ($-2\pi M^2$) always dominates K_{eff} to be negative and no more SRT will happen.

The net K_{eff} as compared with the individual components (such as $B_s\varepsilon_s$, k_s, K_{me}, or $-2\pi M^2$) is really small. Thus, the direction of magnetization is controlled by a small difference between two large opposing contributions [Fig. 5(b)]. Change in any one of the components may thus easily influence the final outcome. From an engineering point of view, this allows us to "tweak" the system one way or another.

B. Comparison between Ni/Cu_3Au(100) and Ni/Cu(100)

Different substrates of Cu(100) and Cu_3Au(100) provide different environments and conditions for the Ni films, such as the film-substrate interface and the lattice mismatch, which implies the different strain. Only the intrinsic properties of Ni films, the magnetic moment density (M) and the magnetoelastic constant ($B_v=K_{\mathrm{me}}^{\mathrm{Ni}}/\mathrm{strain}$) are unchanged, as shown in in Eqs. (7) and (10). Thus, the modification of K_s and K_v by changing the substrate is reasonable. That is also the reason for the different SRT critical thicknesses in the two cases.

As compared with Ni/Cu(100) system, in which $K_v=(K_{\mathrm{me}}-2\pi M^2)\sim 20\ \mu\mathrm{eV/atom}$ (Table I), Ni/Cu_3Au(100) reveals a larger strain, which means a larger $K_v\sim 42\ \mu\mathrm{eV/atom}$ [Fig. 5(b)], about 2.1 times of that in Ni/Cu(100). Accordingly, one might expect the first SRT to occur at much lower coverage in the Ni/Cu_3Au(100) system in comparison with the Ni/Cu(100) system. However, the critical thickness of the first SRT (d_{c1}) in both systems are quite similar. The reason is that, in Figs. 5(c) and 5(d), $K_s(=B_s\varepsilon_s+k_s)\sim -336\ \mu\mathrm{eV/atom}$ in the Ni/Cu_3Au(100) system, about 2.2 times of that in Ni/Cu(100) system ($K_s\sim -154\ \mu\mathrm{eV/atom}$). Since in the thickness region of the first SRT, the strain relaxation is not serious, the above values are taken from the condition without strain relaxation (the value at ~8 ML). Thus, we have the conclusion: Both K_v and K_s are about twice that in the Cu_3Au(100) system relative to the Cu(100) system. According to Eq. (6), the factors of K_s and K_v cancel each other, and there is no apparent difference in the d_{c1} of the two systems.

With regard to the second SRT, d_{c2} of Ni/Cu_3Au(100) is much smaller than that of Ni/Cu(100) (30–70 ML). One reason is the earlier strain relaxation in Ni/Cu_3Au(100), which makes K_{me} drop down earlier. The other reason is the larger negative K_s of Ni/Cu_3Au(100), which can drive K_{eff} negative again even when $K_v=K_{\mathrm{me}}-2\pi M^2$ is still positive (but small). In Ni/Cu(100), K_{eff} goes back to be negative only after $K_v<0$[8].

C. Alloy effect on SRT

In Fig. 5(b), we can see the alloy effect on both K_s/d and K_v. With the higher Co concentration, K_s/d gradually increases and inversely, K_v gradually decreases. This means that, from the view of K_s, increase of the Co concentration x will shift K_{eff} upward and however, in the view of K_v, increase of x will shift K_{eff} downward. The alloy effects on K_s and K_v are opposite to each other. The final result of their competition is the K_{eff} shown in Fig. 5(a), which shifts downward with increasing x. Apparently, alloy effect on the volume anisotropy, especially K_{me}, dominates the final result. We conclude that the delaying of the first SRT and the advancing of the second SRT originate from the strongly reduced K_{me} (or B_v) by Co concentration.

D. Comparison between Co_xNi_{1-x}/Cu_3Au(100) and Co_xNi_{1-x}/Cu(100)

From the inset of Fig. 4, the first SRT boundary was shifted from 7 to more than 20 ML (variation >13 ML) by 9% Co in Cu(100) system. However, in the case of Cu_3Au(100) system (Fig. 4), the shift is only ~2 ML by 9.5% Co. Following the above discussion, we also try to find the reason for the significant difference.

At first, we neglect the strain relaxation during the thickness region of the first SRT and calculate the anisotropy energy at ~8 ML in the two cases.

TABLE II. Comparison between Co_xNi_{1-x}/Cu_3Au(100) and Co_xNi_{1-x}/Cu(100).

	$\frac{K_s^{0\%}}{K_s^{9.4\%}}$	$\frac{K_v^{0\%}}{K_v^{9.4\%}}$	Estimation: $\frac{(K_s^{0\%}/K_s^{9.4\%})}{(K_v^{0\%}/K_v^{9.4\%})}$	Experimental $\frac{d_{c1}^{0\%}}{d_{c1}^{9.4\%}}$
Co_xNi_{1-x}/Cu_3Au(100)	~2	~2	~1	8/10
Co_xNi_{1-x}/Cu(100)	~1	~3	~1/3	7/20

(a) $Cu_3Au(100)$ system: From Figs. 5(c)–5(f), $K_s = B_s\varepsilon_s + k_s$ and $K_v = K_{me} - 2\pi M^2$ are reduced by 9.4% Co from $K_s^{0\%} = -336$ to $K_s^{9.4\%} = -182$ μeV/atom ($K_s^{0\%}/K_s^{9.4\%} \sim 2$) and from $K_v^{0\%} = 42$ (for pure Ni) to $K_v^{9.4\%} = 21$ (for 9.4% Co) μeV/atom ($K_v^{0\%}/K_v^{9.4\%} \sim 2$).

(b) Cu(100) system: From Eq. (7) and Table I K_s and K_v are reduced by 9.4% Co from $K_s^{0\%} = -77$ to $K_s^{9.4\%} = -75$ μeV/atom ($K_s^{0\%}/K_s^{9.4\%} \sim 1$) and from $K_v^{0\%} = 20$ to $K_v^{9.4\%} = 6.2$ μeV/atom ($K_v^{0\%}/K_v^{9.4\%} \sim 3$).

With the above ratios and Eq. (6): $d_c = -K_s/K_v$, we can estimate the ratio of $d_{c1}^{0\%}$ (for pure Ni) to $d_{c1}^{9.4\%}$ (for 9.4% Co) of $Cu_3Au(100)$ and Cu(100) systems to be "1" and "1/3," respectively, which are close to the experimental values: 8 ML/10 ML, and 7 ML/20 ML, respectively. For the ease of comparison, all the related ratios are listed in Table II.

Thus, we can have the following conclusions about the smaller alloy-induced shift of the first SRT in the $Co_xNi_{1-x}/Cu_3Au(100)$ system as compared with $Co_xNi_{-x}/Cu(100)$ system.

(1) Both the larger ($K_s^{0\%}/K_s^{9.4\%}$) ratio and the smaller ($K_v^{0\%}/K_v^{9.4\%}$) ratio in the $Cu_3Au(100)$ system result in the $d_{c1}^{0\%}/d_{c1}^{9.4\%} \sim 1$, being very different from the $d_{c1}^{0\%}/d_{c1}^{9.4\%} \sim 1/3$ in Cu(100) system. Thus, the alloy-induced shift of d_{c1} is much smaller in the $Cu_3Au(100)$ system.

(2) The small deviation between the estimated ratio: $d_{c1}^{0\%}/d_{c1}^{9.4\%} \sim 1$ and the experimental values: $d_{c1}^{0\%}/d_{c1}^{9.4\%} \sim 8/10$ in the $Cu_3Au(100)$ system is due to the neglecting of strain relaxation, which results in reduction of $B_s\varepsilon_s$, and thus induces ~ 2 ML shift of d_{c1}.

(3) The earlier strain relaxation in the $Cu_3Au(100)$ system is not the main reason for the significant difference between the first SRT of the $Cu_3Au(100)$ and Cu(100) systems. In Figs. 5(c) and 5(d), because k_s dominates in the surface anisotropy (K_s), the quick decay of $B_s\varepsilon_s$ driven by strain relaxation thus does not cause a significant shift of the d_{c1} for the SRT. As mentioned in Point 2, the strain-related terms only induce ~ 2 ML shift of d_{c1}.

VI. SUMMARY

The $Co_xNi_{1-x}/Cu_3Au(100)$ alloy films with x up to 11% revealed the same growth behaviors as pure Ni films on $Cu_3Au(100)$. Layer-by-layer growth persisted up to 5 ML and then the amplitude of the MEED oscillation was quickly reduced to a smaller value. Further decay of the small-amplitude oscillation proceeded slowly and the oscillations were sustained at least up to 20 ML. In LEED-I/V curves, the thickness-dependent strain relaxation was observed to follow a common trend. No significant difference appeared when the alloy composition was varied ($x \leqslant 11\%$). For magnetic properties, the strain-induced first and second SRT were measured by MOKE within 20 ML. Alloy composition influenced the SRT behavior significantly. Increasing the Co concentration strongly reduced the thickness region for perpendicular magnetization. By combining the alloy effect and the strain relaxation effect in a phenomenological model on the basis of magnetoelastics, the SRT boundary in the phase diagram can be fit well with the experimentally measured thickness-dependent strain profile. This result depicts the thickness evolution and the alloy modification of distinct magnetic anisotropy terms. From the detailed evolution of anisotropy energy, the following conclusions are given.

(1) Strain-induced (thickness-dependent) SRT: When <10 ML, the positive K_{me} and the fast reducing K_s/d (<0) result in the first SRT. After 10 ML, due to the strain relaxation, K_{me} drops down quickly and is covered by negative K_s/d. Thus, the second SRT happens.

(2) Comparison between $Ni/Cu_3Au(100)$ and Ni/Cu(100): Since K_s and K_v are both about twice as large in the $Ni/Cu_3Au(100)$ system relative to those of the Ni/Cu(100) system, according to Eq. (6), there is no apparent difference in d_{c1} of both systems. Due to the earlier strain relaxation and the larger negative K_s, d_{c2} of $Ni/Cu_3Au(100)$ is much smaller than that of Ni/Cu(100).

(3) Alloy effect on SRT: The delayed first SRT and the advanced second SRT originate from the strongly reduced K_{me} (or B_v) by introduction of Co.

(4) Comparison between $Co_xNi_{1-x}/Cu_3Au(100)$ and $Co_xNi_{1-x}/Cu(100)$: Both the larger $K_s^{0\%}/K_s^{9.4\%}$ and the smaller $K_v^{0\%}/K_v^{9.4\%}$ in the $Cu_3Au(100)$ system drive the $d_{c1}^{0\%}/d_{c1}^{9.4\%} \sim 1$, very different from the $d_{c1}^{0\%}/d_{c1}^{9.4\%} \sim 1/3$ in Cu(100) system. Thus, the alloy-induced shift of d_{c1} is much smaller in $Cu_3Au(100)$ system.

ACKNOWLEDGMENTS

This work was supported by the National Science Council under Grant Nos. NSC 92-2112-M-002-019 and NSC 92-2112-M-001-039, MOEA program (Grant No. 92-EC-17-A-08-S1-0006), and the Ministry of Education of Taiwan. We also thank Dr. J. C. Lin of IAMS, who kindly provided us an energy analyzer for our Auger studies.

*Electronic address: song@po.iams.sinica.edu.tw

†Author to whom correspondence should be addressed; electronic address: mtlin@phys.ntu.edu.tw

[1] W. C. Lin, C. C. Kuo, C. L. Chiu, and M.-T. Lin, J. Appl. Phys. **89**, 7139 (2001).

[2] M.-T. Lin, J. Shen, W. Kuch, H. Jenniches, M. Klaua, C. M. Schneider, and J. Kirschner, Phys. Rev. B **55**, 5886 (1997).

[3] R. Allenspach, M. Stampanoni, and A. Bischof, Phys. Rev. Lett. **65**, 3344 (1990).

[4] S. Müller, P. Bayer, C. Reischl, K. Heinz, B. Feldmann, H. Zillgen, and M. Wuttig, Phys. Rev. Lett. **74**, 765 (1995).

[5] M.-T. Lin, J. Shen, W. Kuch, H. Jenniches, M. Klaua, C. M. Schneider, and J. Kirschner, Surf. Sci. **410**, 290 (1998).

[6] B. Feldmann, B. Schirmer, A. Sokoll, and M. Wuttig, Phys. Rev.

B **57**, 1014 (1998).
[7] F. Huang, M. T. Kief, G. J. Mankey, and R. F. Willis, Phys. Rev. B **49**, 3962 (1994).
[8] Gabriel Bochi, C. A. Ballentine, H. E. Inglefield, C. V. Thompson, and R. C. O'Handley, Phys. Rev. B **53**, R1729 (1996).
[9] B. Schulz and K. Baberschke, Phys. Rev. B **50**, 13 467 (1994).
[10] W. L. O'Brien, T. Droubay, and B. P. Tonner, Phys. Rev. B **54**, 9297 (1996).
[11] R. Jungbult, M. T. Johnson, J. a. d. Stegge, A. Reinders, and F. J. A. d. Broeder, J. Appl. Phys. **75**, 6424 (1994).
[12] A. Dittschar, W. Kuch, M.-T. Lin, C. M. Schneider, and J. Kirschner, Phys. Rev. B **57**, R3209 (1998).
[13] R. Thamankar, A. Ostroukhova, and F. O. Schumann, Phys. Rev. B **66**, 134414 (2002).
[14] C. C. Kuo, S. F. Chuang, W. Pan, W. C. Lin, and M.-T. Lin, J. Appl. Phys. **91**, 7185 (2002); C. C. Kuo, W. C. Lin, S. F. Chuang, and M.-T. Lin, Surf. Sci. (to be published).
[15] Minn-Tsong Lin, W. C. Lin, C. C. Kuo, and C. L. Chiu, Phys. Rev. B **62**, 14 268 (2001).
[16] P. James, O. Eriksson, O. Hjaortstam, B. Johansson, and L. Nordström, Appl. Phys. Lett. **76**, 915 (2000).
[17] A. Lessard, T. H. Moos, and W. Hübner, Phys. Rev. B **56**, 2594 (1997).
[18] P. James, O. Eriksson, B. Johansson, and I. A. Abrikosov, Phys. Rev. B **59**, 419 (1999).
[19] W. C. Lin, C. C. Kuo, C. L. Chiu, and M.-T. Lin, Surf. Sci. **478**, 9 (2001).
[20] F. Matthes, M. Scider, and C. M. Schneider, J. Appl. Phys. **91**, 8144 (2002).
[21] A. Braun, B. Feldmann, and M. Wuttig, J. Magn. Magn. Mater. **171**, 16 (1997).
[22] A. Enders, D. Sander, and J. Kirschner, J. Appl. Phys. **85**, 5279 (1999).
[23] K. Ha, M. Ciria, R. C. O'Hanhley, P. W. Stephens, and S. Pagola, Phys. Rev. B **60**, 13 780 (1999).
[24] W. Platow, U. Bovensiepen, P. Poulopoulos, M. Farle, K. Babschke, L. Hammer, S. Walter, S. Müller, and K. Heinz, Phys. Rev. B **59**, 12 641 (1999).
[25] This analytical function is just used to reproduce the experimental data as a continuous function of the film thickness. It is for the convenience in the fitting of SRT boundary described later in the text.
[26] M. Kowalewski, C. M. Schneider, and B. Heinrich, Phys. Rev. B **47**, 8748 (1993).
[27] R. F. Willis, J. A. C. Bland, and W. Schwarzacher, J. Appl. Phys. **63**, 4051 (1988).
[28] C. Kittel, *Introduction to Solid State Physics*, 7th ed. (Wiley, New York, 1996), p. 457.
[29] This is due to the fact that if $\varepsilon_s=\varepsilon_v$ is the dotted line in Fig. 2(b), the residual strain after 16 ML will be $\sim$1% and changes slowly with thickness. This residual strain leads the volume magnetoelastic anisotropy K_{me} of pure Ni$\sim$9 μeV/atom, very close to the absolute value of the shape anisotropy. So, the denominator of Eq. (6) approaches zero after 16 ML, and then the d_{c2} becomes very large, which means a long tail in the boundary of the second SRT (dashed line in Fig. 4).
[30] Since the B_{s1} is multiplied by both surface strain ($\leqslant$6%) and alloy concentration ($\leqslant$11%), B_{s0} is multiplied by surface strain, and k_{s1} is multiplied by the alloy concentration in Eq. (10), their values and errors are larger than k_{s0} by two or one magnitudes of order.
[31] Bochi's $B_s=15$ erg/cm$^2=6105$ μeV/atom and a factor of ($-1/1.18$) are added according to Eq. (2), because we choose $\varepsilon_s=\varepsilon_\perp$, and they choose $\varepsilon_s=\varepsilon_\parallel$.